Electronic Supplementary Material (ESI) for Materials Advances.

White Light Emitting Silsesquioxane Based Materials: the Importance of a Ligand with Rigid and Directional Arms

*Andrea Santiago-Portillo,[a] Valerio Cinà,[a,b] Esther Carbonell,[a] Luca Fusaro,[a] Vincent Lemaur,[c] Roberto Lazzaroni,[c] Michelangelo Gruttadauria,[b] Francesco Giacalone,[*b] Carmela Aprile [*a]*

[a] Unit of Nanomaterial Chemistry (CNano), Department of Chemistry, University of Namur, Rue de Bruxelles 61, 5000, Namur, Belgium.

[b] Department of Biological, Chemical and Pharmaceutical Sciences and Technologies, University of Palermo, Viale delle Scienze, Ed.17, 90128, Palermo, Italy.

[c] Laboratory for Chemistry of Novel Materials, Materials Research Institute, University of Mons-UMONS, Place du Parc 20, Mons B-7000, Belgium.

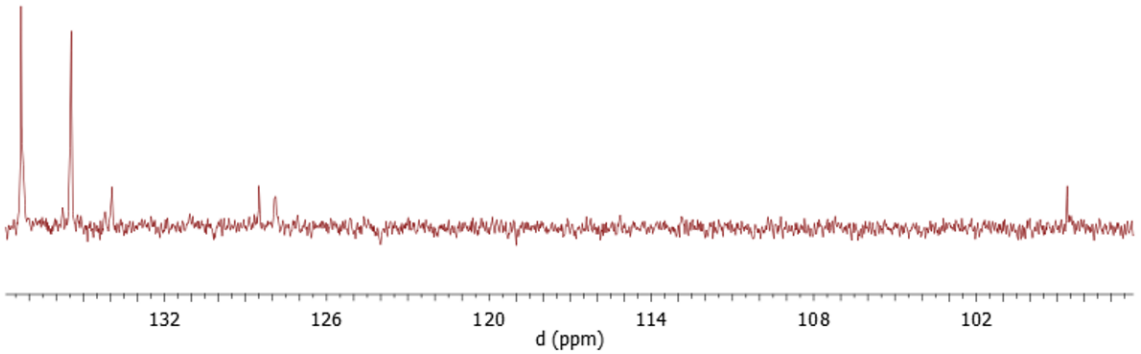

Figure S1. ^{13}C NMR spectrum of I-POSS (101 MHz, THF).

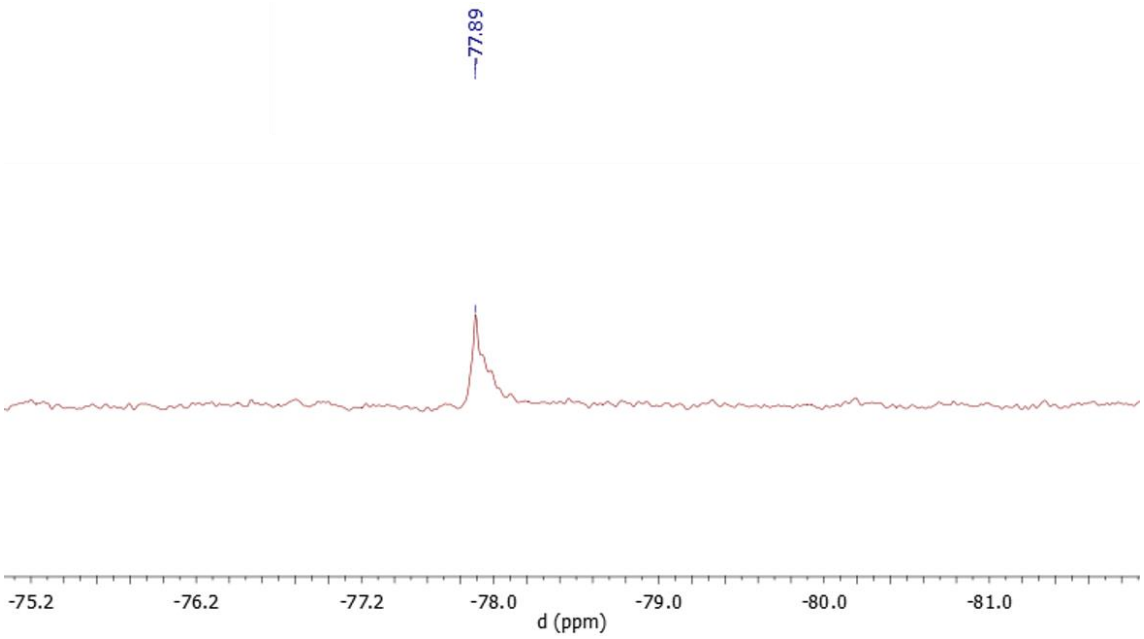

Figure S2. ^{29}Si NMR spectrum of I-POSS (79 MHz, THF).

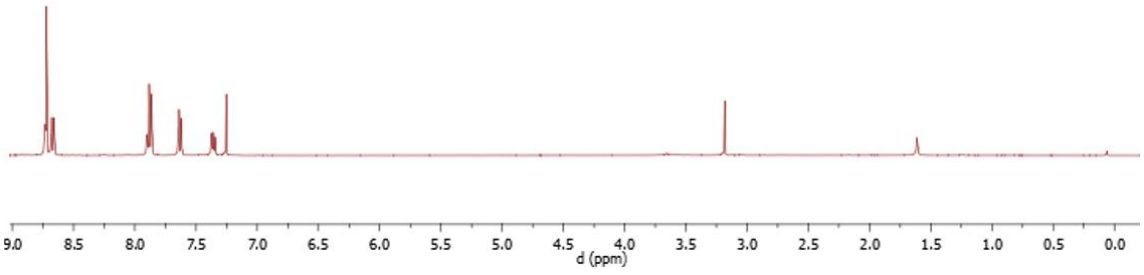

Figure S3. ^{1}H NMR spectrum of 4'-(4-Ethylnylphenyl)-[2,2':6,2'']terpyridine (300 MHz, $CDCl_3$).

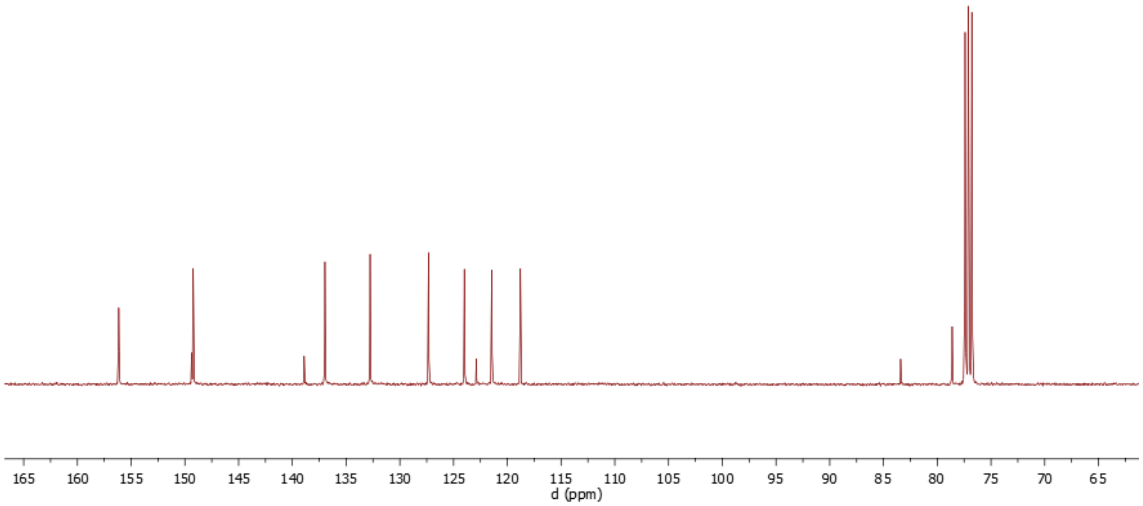

Figure S4. ^{13}C NMR spectrum ($CDCl_3$) of 4'-(4-Ethylnylphenyl)-[2,2':6,2'']terpyridine (101 MHz, $CDCl_3$).

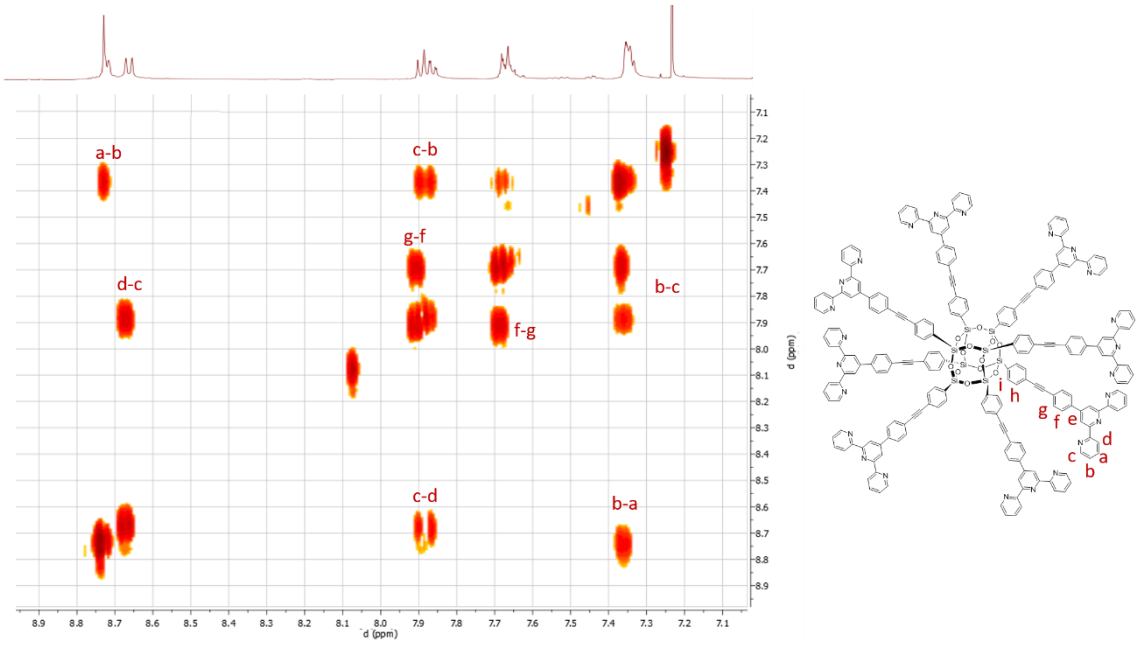

Figure S5. COSY NMR spectrum ($CDCl_3$) of Ter-POSS.

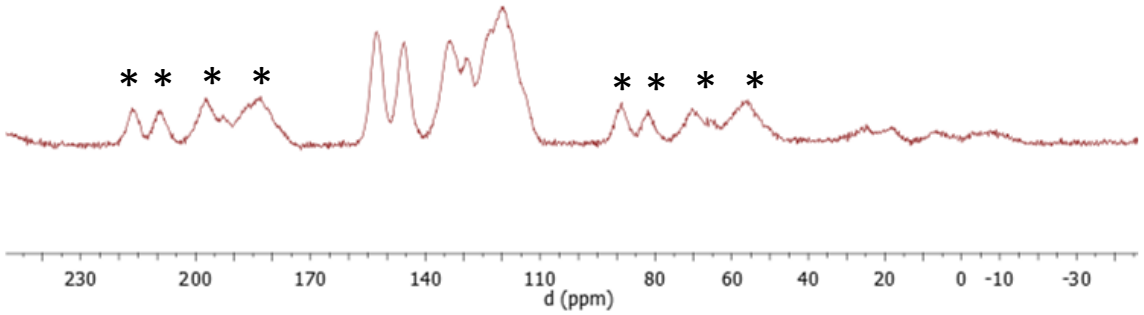

Figure S6. CP-MAS ^{13}C NMR spectrum of Ter-POSS in solid-state (125 MHz, 8kHz). Asterisks denote spinning sidebands.

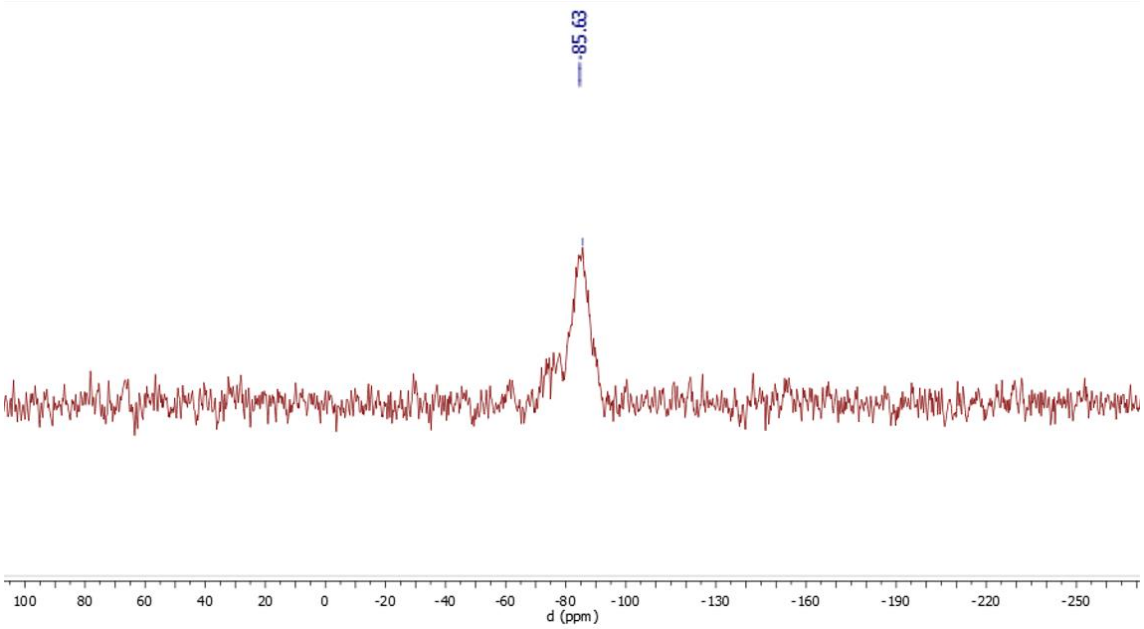

Figure S7. CP-MAS ^{29}Si NMR spectrum of Ter-POSS in solid-state (99.3 MHz, 8kHz).

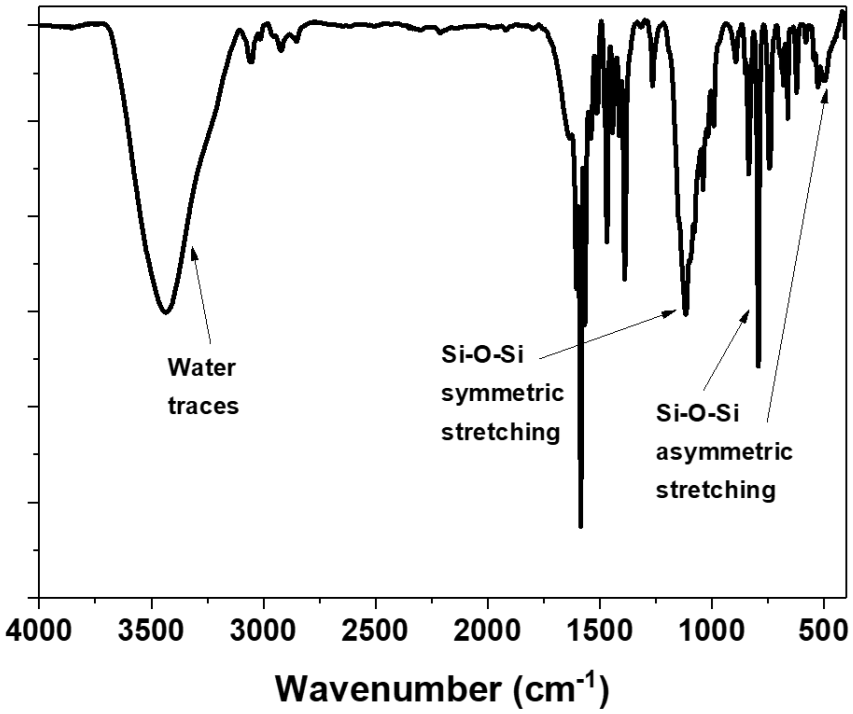

Figure S8. IR spectrum Ter-POSS.

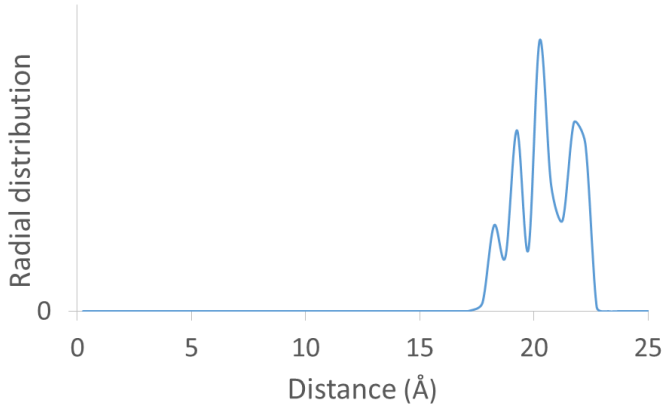

Figure S9. Radial distribution function between the nitrogen atoms of the central pyridine ring in different terpyridine arms of Ter-POSS. The graph has been built from 1000 structures generated during a 10-ns MD run at room temperature.

The results of the calculations for O-POSS are presented in Figure S10. Interestingly, the most stable structure exhibits five arms with a Z-conformation around the double bond and three arms with a E-conformation. Such combination allows for strong interactions between some terpyridine groups, as revealed by the radial distribution function analysis, with distances that can be as small as 5 Å. Strong interactions between the terpyridine groups are also found for the Z-isomer while the E-isomer, with its fully

extended arms, only exhibits weak interactions. Even though the E-isomer ressembles Ter-POSS, here, contacts at smaller distances are allowed due to the higher flexibility of the arms.

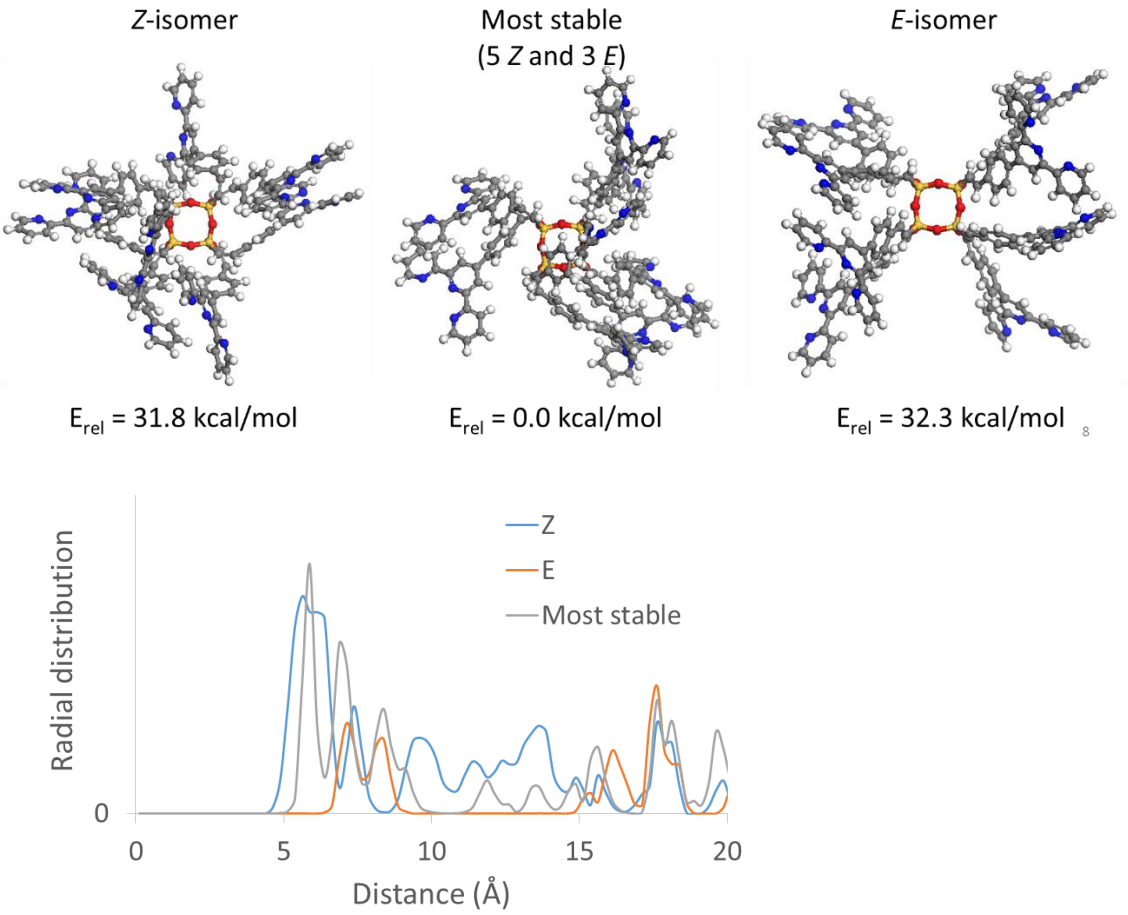

Figure S10. Top: representation of the most stable structures of O-POSS and their relative energies (in kcal/mol). Bottom: radial distribution function between the nitrogen atoms of the central pyridine ring in different terpyridine arms. The graphs have been built from 1000 structures generated during a 10-ns MD at room temperature.

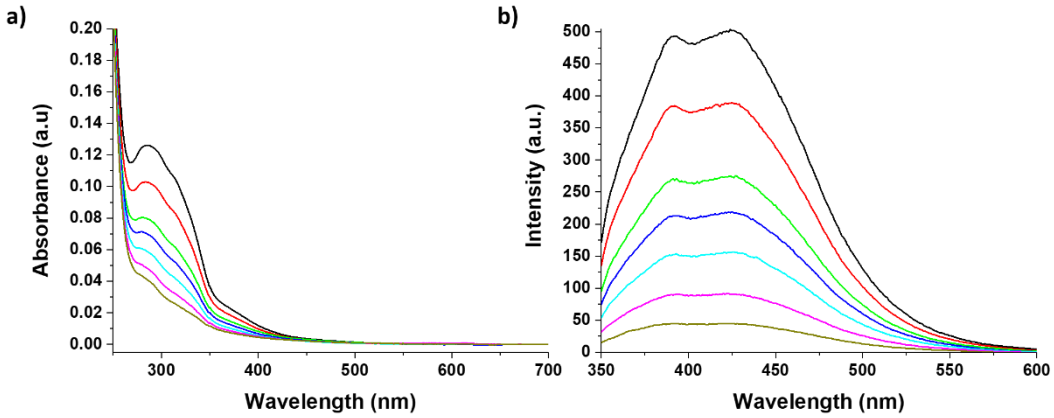

Figure S11. (a) UV-vis Absorption spectra of Ter-POSS in CH_2Cl_2 in different concentrations. (b) Emission spectra of Ter-POSS. λ_{ex} = 330 nm, Slits = 10 nm.

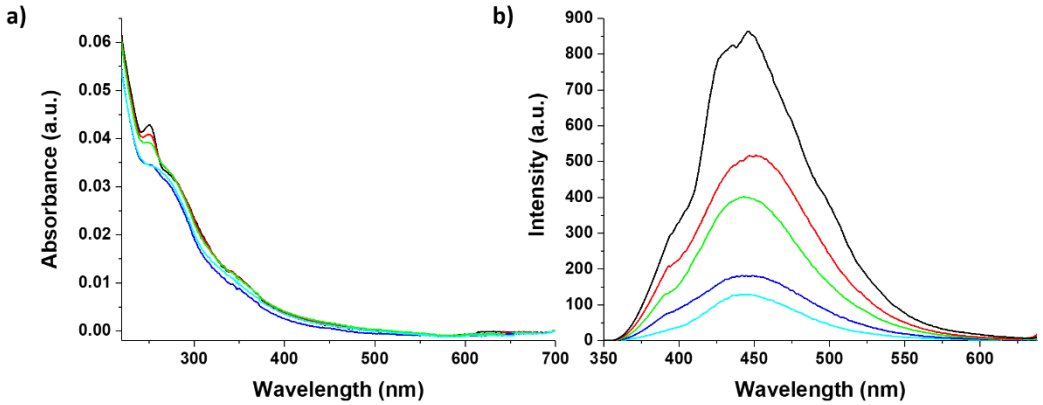

Figure S12. (a) UV-vis Absorption spectra of Quinine Sulfate in 0.1M H_2SO_4 in different concentrations. (b) Emission spectra of Quinine sulfate. λ_{ex} = 330 nm, Slits = 10 nm.

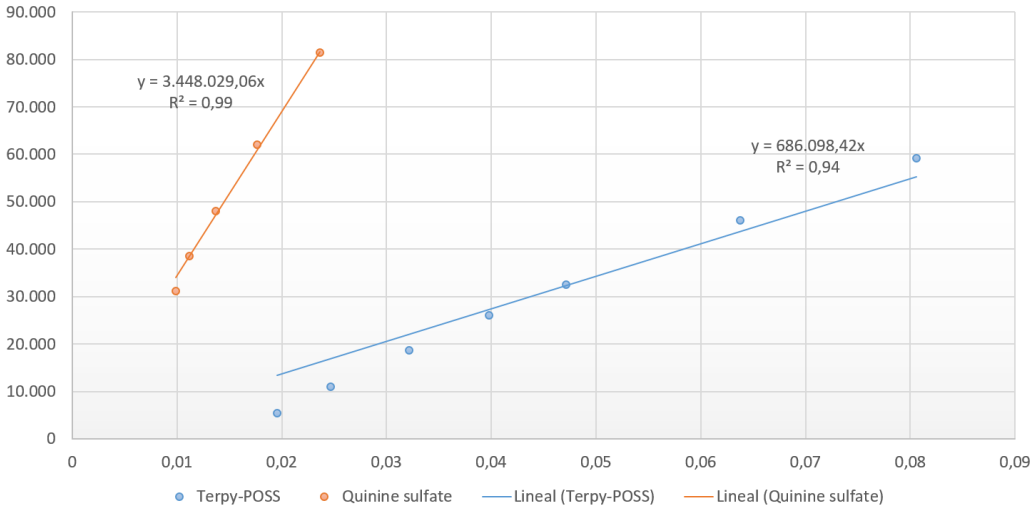

Figure S13. Quantum yield Ter-POSS. The graph reports the fluorescence intensity (y) *vs* the absorption intensity at excitation wavelength (x).

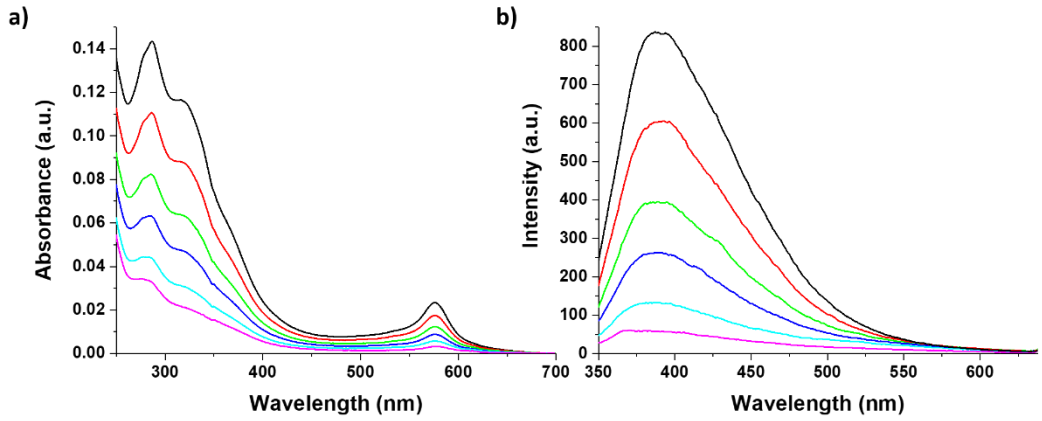

Figure S14. (a) UV-vis Absorption spectra of Ter-POSS@4Fe in CH_2Cl_2 in different concentrations. (b) Emission spectra of Ter-POSS@4Fe. λ_{ex} = 330 nm, Slits = 10 nm.

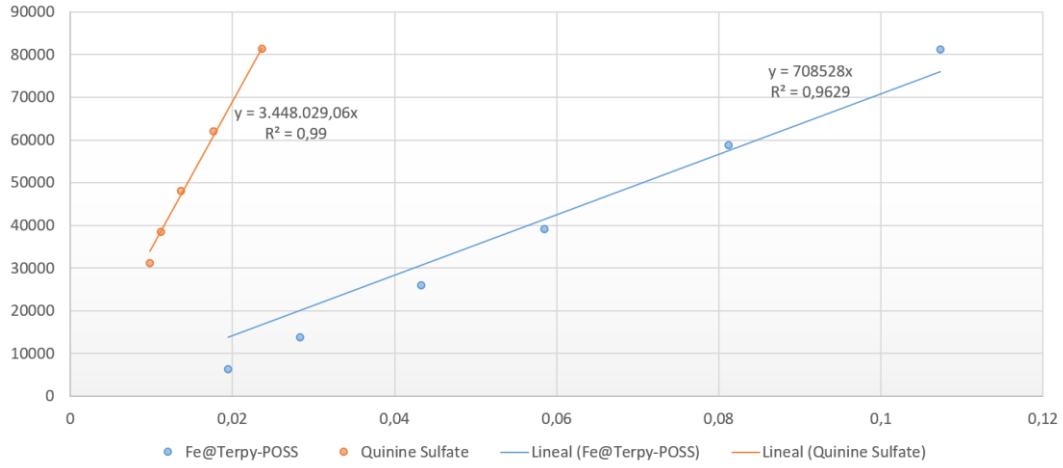

Figure S15. Quantum yield Ter-POSS@4Fe. The graph reports the fluorescence intensity (y) *vs* the absorption intensity at excitation wavelength (x).

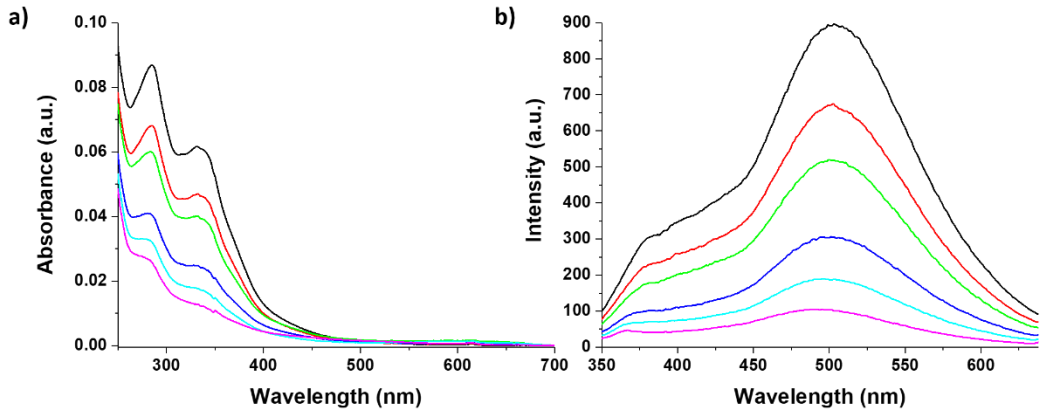

Figure S16. (a) UV-vis Absorption spectra of Ter-POSS@4Zn in CH_2Cl_2 in different concentrations. (b) Emission spectra of Ter-POSS@4Zn. λ_{ex} = 330 nm, Slits = 10 nm.

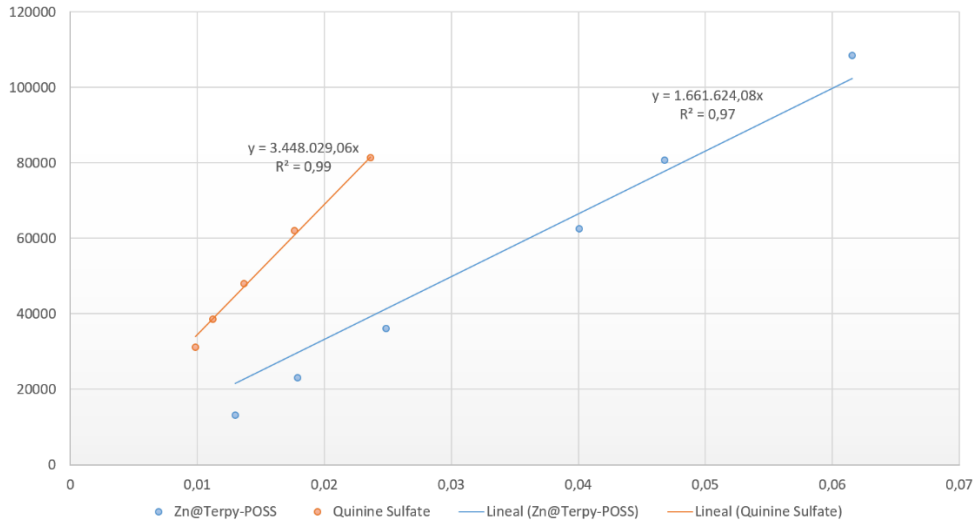

Figure S17. Quantum yield Ter-POSS@4Zn. The graph reports the fluorescence intensity (y) *vs* the absorption intensity at excitation wavelength (x).

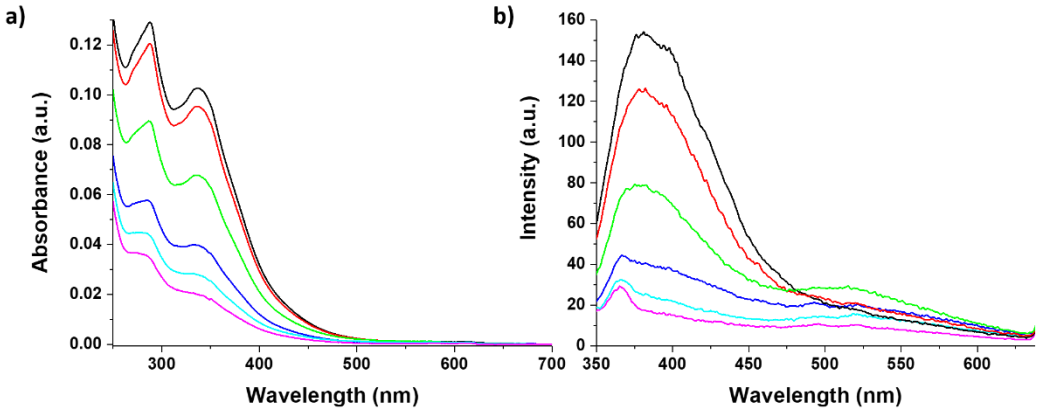

Figure S18. (a) UV-vis Absorption spectra of Ter-POSS@4Cu in CH_2Cl_2 in different concentrations. (b) Emission spectra of Ter-POSS@4Cu. λ_{ex} = 330 nm, Slits = 10 nm.

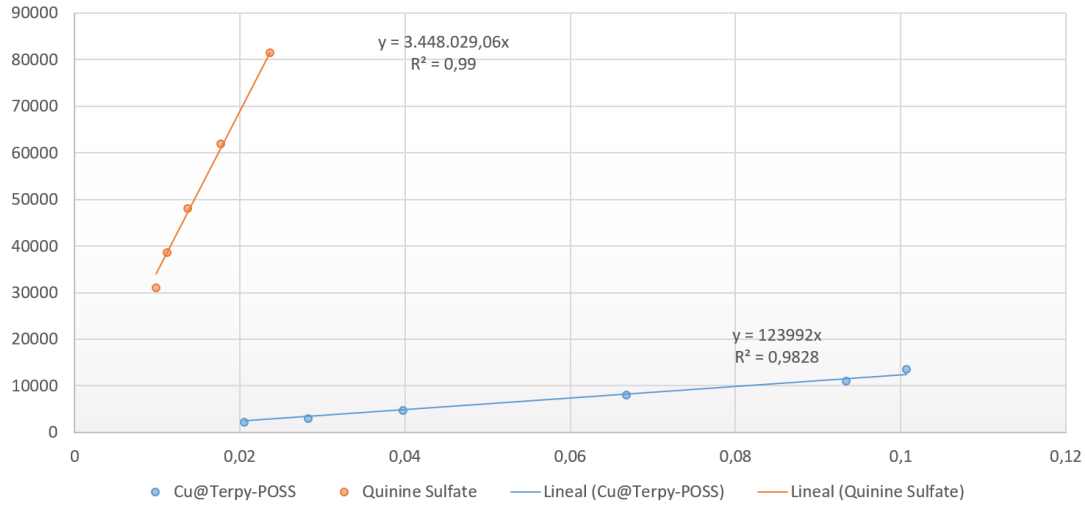

Figure S19. Quantum yield Ter-POSS@4Cu. The graph reports the fluorescence intensity (y) *vs* the absorption intensity at excitation wavelength (x).

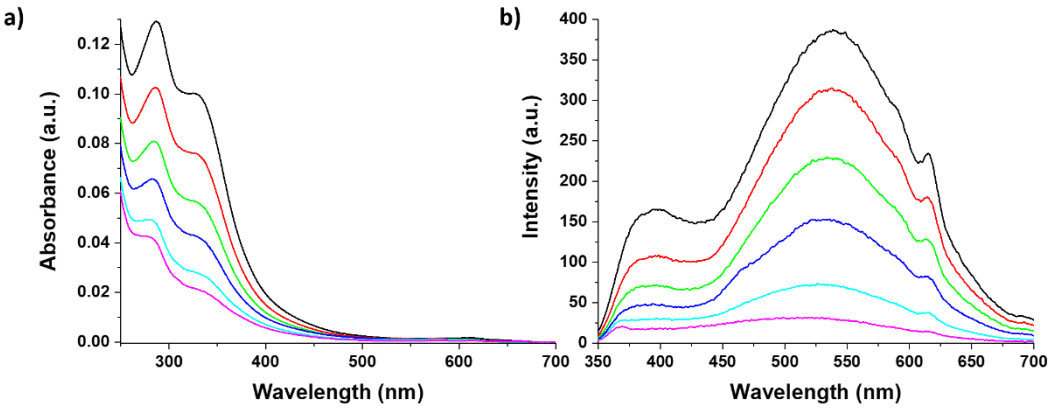

Figure S20. (a) UV-vis Absorption spectra of Ter-POSS@4Eu in CH_2Cl_2 in different concentrations. (b) Emission spectra of Ter-POSS@4Eu. λ_{ex} = 330 nm, Slits = 10 nm.

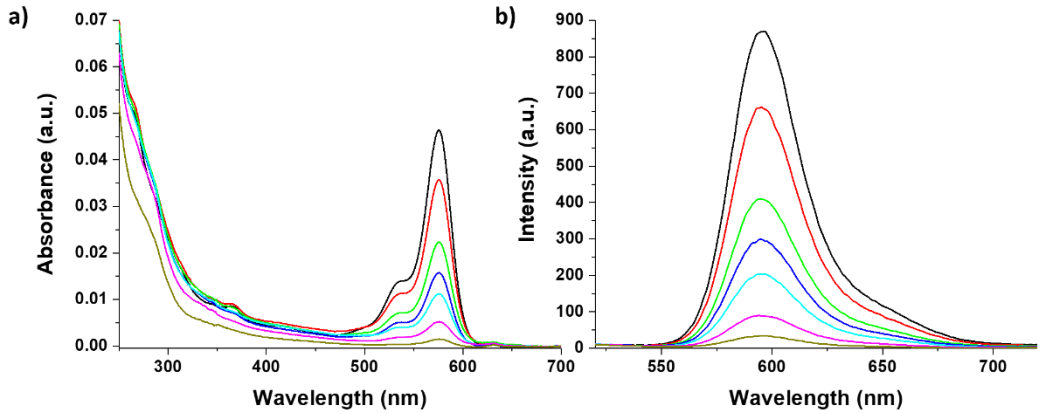

Figure S21. (a) UV-vis Absorption spectra of Rhodamine 101 in ethanol + 0.01% HCl in different concentrations. (b) Emission spectra of Rhodamine 101. λ_{ex} = 330 nm, Slits = 10 nm.

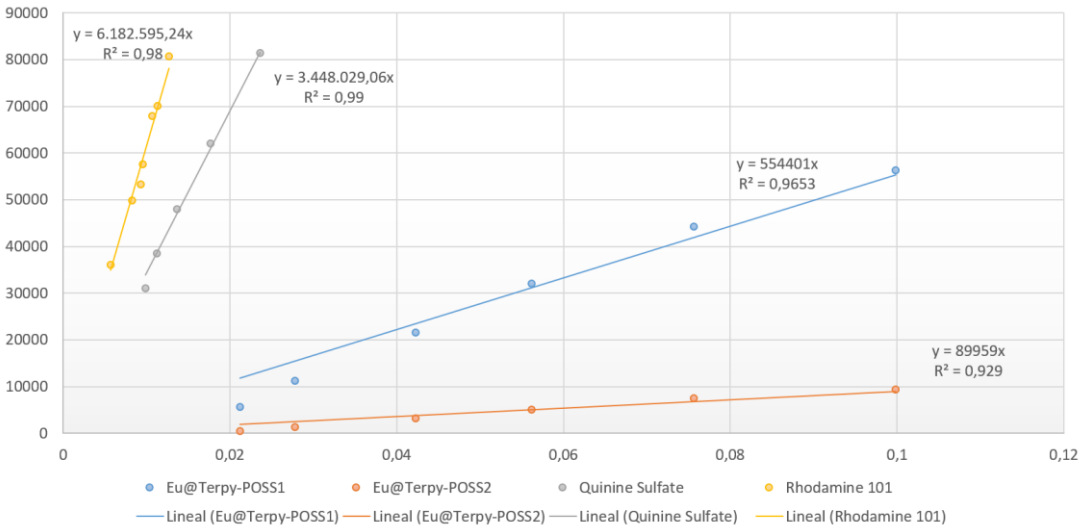

Figure S22. Quantum yield Ter-POSS@4Eu. The graph reports the fluorescence intensity (y) *vs* the absorption intensity at excitation wavelength (x).

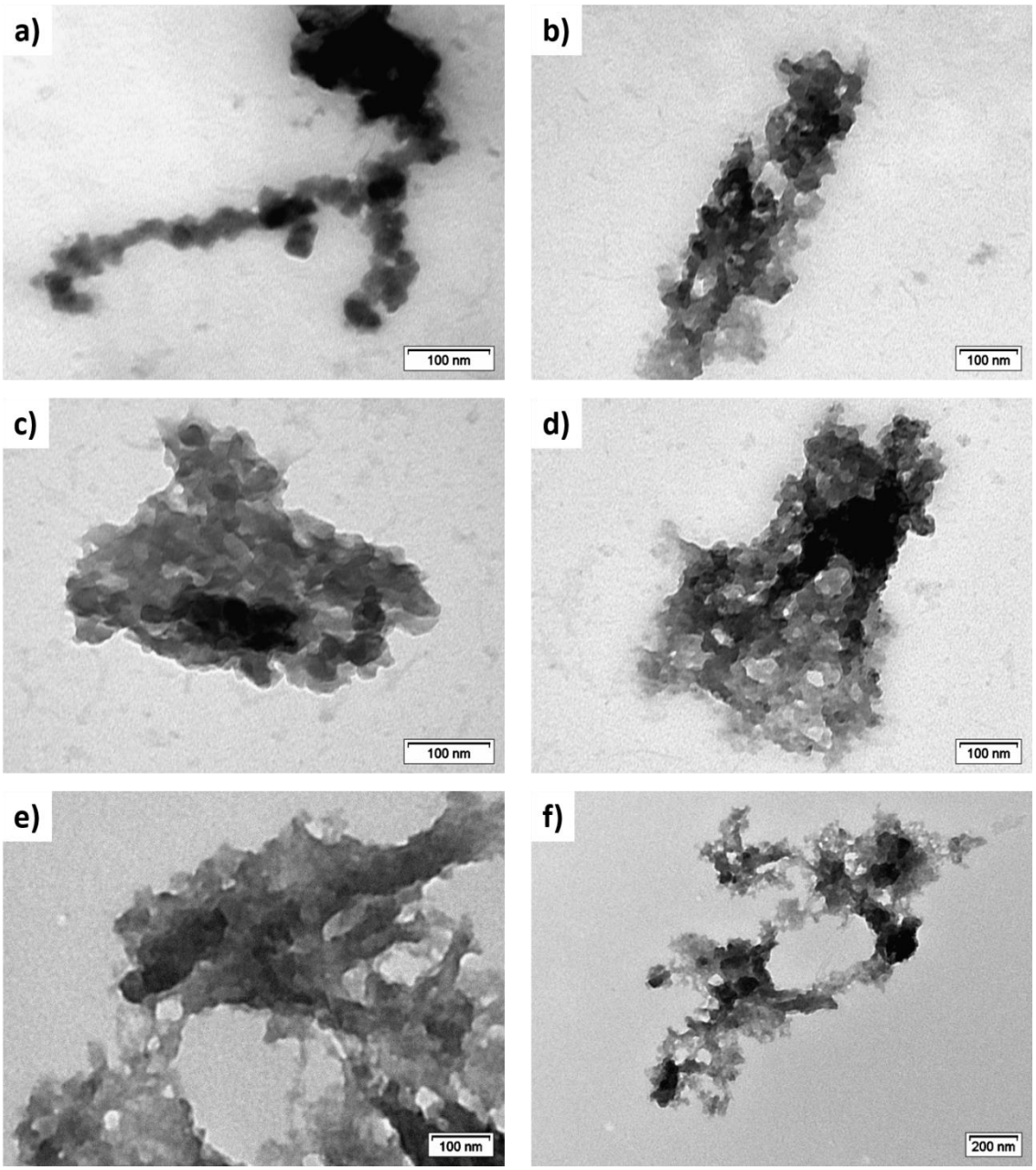

Figure S23. Transmission Electron Microscopy images of the lyophilized Ter-POSS@4Zn (a and b), Ter-POSS@4Cu (c and d) and Ter-POSS@4Eu (e and f).